Materials Science-Poland, *Vol. 27*, *No. 1*, *2009*

Characterization of oxidic and organic materials with synchrotron radiation based XPS and XAS*

D. SCHMEISSER[1**], M. TALLARIDA[1], K. HENKEL[1], K. MÜLLER[1], D. MANDAL[1], D. CHUMAKOV[2], E. ZSCHECH[2]

[1]Applied Physics Sensors, Brandenburg Technical University Cottbus, 03046 Cottbus, Konrad-Wachsmann-Allee 17, Germany

[2]AMD Saxony, Wilschdorfer Landstr. 101, 01109 Dresden, Germany

The use of synchrotron radiation (SR) based X-ray absorption spectroscopy (XAS) and X-ray induced photoelectron spectroscopy (XPS) is demonstrated for the analysis of thin films. In the first part we report on oxidic films used for high-*k* dielectric films in Si technology and focus on a recent in-situ approach to study the atomic layer deposition growth of HfO_2 films. We demonstrate that even hidden layers can be characterized by using fluorescence technologies. In the second part, we demonstrate the suitability of SR based techniques for the analysis of organic thin films. Here, the first example deals with P(VDF-TrFE), a ferroelectric polymer, with possible applications in non-volatile memory devices. Another example concerns the analysis of C_{60} based low-*k* polymers for use in Cu interconnect systems.

Key words: *synchrotron radiation spectroscopy; HfO_2; high-k oxide; ultralow-k polymers*

1. Introduction

Analysis of materials using synchrotron based spectroscopy techniques is a field with many possible applications. The main field of research in our group at the BTU Cottbus is in the materials science of thin functional films [1]. In our studies, we combine both, electrical and spectroscopic studies for their characterization. We have focused on two classes of materials, oxidic thin films – some of which are used as high-*k* dielectrics in MIS stacks and on organic thin films – some of which are used as low-*k* dielectrics to isolate around Cu interconnects.

We have prepared thin films of Pr_2O_3 and HfO_2 on Si and SiC substrates to build MIS structures for their electrical characterization. We optimized the films in terms of

---

* Presented at the 3rd Workshop *Hybrid Nanostructured Materials*, Prague, Czech Republic, 5–6 November, 2007.

**Corresponding author, e-mail: dsch@tu-cottbus.de

their dielectric properties (k value) and their insulating properties (leakage current densities). In particular, we stress that the studied oxide films are always controlled in their stoichiometry and thickness by spectroscopic means [2–10].

The intrinsic properties of the oxide thin films are monitored by XPS when optimizing the deposition parameters. This ensures control over stoichiometry, phase stability, and defined film thickness. Another investigation controls the temperature stability of the deposited oxide films. Such studies were done for pure but also for some mixed oxide systems [11–14].

Our studies concerned, in particular, the interface stabilities of the ultra thin oxide layers. The interface towards the metal electrodes turned out to be very important, as most metals penetrate into the oxides upon mild annealing. We observed a high mobility of Au, Ag, and Al which could be controlled only by the insertion of a thin Ti diffusion barrier [15].

Interface reactions also occur on the interface towards the substrates. Here in particular the mobility of Si is crucial and causes the formation of silicates [16, 17]. This turned out to be the case for Pr_2O_3 as well as for HfO_2 and Al_2O_3 thin films.

In our systems, we always combine the spectroscopically controlled films with electrical characterization (capacitance–voltage (CV) and current–voltage (IV) measurements). With both approaches, we learned that the introduction of an AlON layer as a buffer layer between the Si substrate and a high-k oxide delivers much better properties than those obtained for the bare system. In particular, the thickness of a silicate rich interface layer could be reduced significantly [4, 15, 18–20].

2. Experimental

Our synchrotron radiation (SR) based spectroscopic studies are performed using the BTU owned beam line U49/2 at BESSY, Berlin [1]. We briefly describe the most important features of the two main techniques applied.

X-ray induced photoemission spectroscopy (XPS) enables a quantitative determination of the elements contained in an investigated sample. The technique may be used with synchrotron radiation (SR) or laboratory X-ray sources. For low-k materials and for organic films in general, this technique is very promising because of the ease of sample preparation. Also, this technique does not suffer from X-ray induced radiation damage. The advantage of using SR as an excitation source is the higher sensitivity and better energy resolution. The higher sensitivity arises from the fact that the photo ionization cross sections are largest close to the ionization threshold. Hence, by using a tunable X-ray source, the excitation energy can be optimized.

The XAS technique again needs a tunable X-ray source, and therefore, this technique is exclusively used at synchrotron radiation sources. Very conveniently, the element-specific absorption coefficient can be determined by recording the total current of the emitted photoelectrons by tuning the energy of the incident photons around a particular ionization threshold (absorption edge). The most intense signal appears

near the absorption edge, the respective technique is referred to as near-edge absorption fine structure spectroscopy (NEXAFS). The method is more bulk-sensitive compared with XPS, since the total photoyield is primarily determined by the secondary electrons. Their mean free path is larger (up to 10 nm) than that of typical XPS photoelectrons. Thereby, the analysis of thicker films is feasible. The absorption coefficient can be determined either by recording the total electron yield (TEY) or by the total fluorescence yield (TFY). Using TFY, even higher bulk-sensitivity is obtained, as the X-ray photons are significantly less attenuated when penetrating through the films. The TFY mode can be beneficial when analyzing oxidic materials, as this mode is less sensitive to sample charging than the TEY mode. Elemental composition can be analyzed quantitatively in thin films. The technique is often used to analyze the chemical bonding, as the shape of the absorption profile differs characteristically for different oxidation states (finger printing) of inorganic compounds. In particular, the XAS spectra of transition and rare earth oxides show very sharp and structured features which can be used to analyze the particular charge state of the atom investigated. Because of the high sensitivity, such studies can also be performed on diluted or mixed oxide systems.

Electrical measurements have been carried out on MIS capacitors at room temperature in dark conditions. For further details of the MIS stack preparation refer to [20]. CV and conductance–voltage (GV) characteristics have been recorded with an Agilent 4284 LCR meter. IV characteristics were recorded using Agilent E3649A, HP34401, PREMA4001 and/or Keithley487 meters, respectively. Permittivity and capacitance equivalent thickness (CET) values were deduced from the oxide capacitance in the accumulation regime of the CV loop. Densities of interface states (D_{it}) were determined by AC conductance maxima [21].

3. Oxidic thin films

3.1. In-situ ALD setup for synchrotron radiation based spectroscopy

Among the possible growth methods, atomic layer deposition (ALD) is the most promising when considering very thin films conformal to three dimensionally structured substrates. As this is the typical request in the newest DRAM technology node, where thin capacitors have a very high aspect ratio (up to 60:1), the ALD growth method has an important industrial potential.

ALD growth contrasts with the chemical vapour deposition (CVD) technique, both of which are frequently used for the preparation of ultra-thin functional films. In both methods, two or more precursors react with each other, producing the targeted material. The difference between the two methods is that the ALD is based on a self-limiting process characterized by the adsorption of the metal precursor on the surface of a substrate. As a consequence of that surface reaction a layer-by-layer growth is achieved. On the other hand, in the CVD growth, the reactions take place in the gas

phase and are not controlled by the surface. Here, it has to be noted that the layer-by -layer growth of ALD does not necessarily correspond to one layer after every cycle but in most of the cases one layer is achieved after several cycles, as the surface coverage at every metal precursor exposure is usually not complete.

The ALD growth of metal oxides consists in the chemisorption of the metal precursor onto the substrate and the subsequent oxidization of the chemisorbed species. The two steps are separated by the introduction of a purging inert gas, which is needed to remove the non-reacted molecules of the metal precursor and the byproduct of the reacted molecules. In this way, with the introduction of the oxidant, the reactions take place only at the surface of the substrate, avoiding the CVD growth.

Up to now most of the investigations of ALD grown, high-*k* films were made ex situ, with the samples prepared in the ALD reactor and analyzed in a separated chamber, implying the transportation in air. This procedure involves the contamination of the high-*k* film and in some cases the formation of SiO_2 in very thin films, which make the interpretation of the experimental results difficult [22]. We show here the first results of our in-situ experiments, where the ALD reactor (base pressure 2×10^{-7} mbar) and the measurement UHV chamber (2×10^{-10} mbar) were connected together through an interface chamber maintained at an intermediate pressure of about 2×10^{-9} mbar. With respect to the ex situ experiments, our procedure assures the measurement of contamination-free surfaces. There is another important advantage of making measurements in situ: with our equipment we can study the film after every cycle and also after any single step of every cycle. This could be important for studying in detail the most important deposition step represented by the oxidation of the chemisorbed metal precursor.

The results presented here were obtained by using $HfCl_4$ as a metal precursor and H_2O as an oxidant, while the purging gas was N_2. The pressure reached by the metal precursor was 2×10^{-5} mbar and that of H_2O was 2×10^{-2} mbar, with one cycle consisting of 6 min exposure to $HfCl_4$ and 20 s exposure to H_2O, with a purging time of 2 min. After the oxidation step, another purging exposure was made before moving the sample into the interface chamber. The maximum value of deposition rate found for the ALD growth with the $HfCl_4$ as a metal precursor is about 1 ML every 3 cycles [23]. The temperature of the Si substrate was maintained at 300 °C during the complete cycle, and the ALD reactor was maintained at 140 °C during the experiment to avoid the condensation of $HfCl_4$ on the walls of the reactor. The $HfCl_4$ source was heated also at ca. 140 °C during the metal precursor step and then fast cooled to about 50 °C. The Si(001) substrate was cut from an n-type doped wafer, covered with a 2.2 nm thick oxide. The oxide was partially removed by etching the sample in a diluted HF solution, leaving the surface with an OH group termination. The remaining oxide thickness was determined to be 0.5 nm by the relative intensity of the peaks of the Si^{0+} and Si^{4+} species in the Si2p core level.

The photoemission and NEXAFS experiments were all performed at the synchrotron source BESSY in Berlin, at the beam line U49/2. The synchrotron light can be

made to have high photon intensity in a wide range of energy, leading to a high surface sensitivity and high energy resolution of the photoemission experiments, much higher compared with the usual AlK_α lab source. This is important because the films under investigation are of the order of less than a few nanometers and a detailed analysis requires both high sensitivity and good energy resolution.

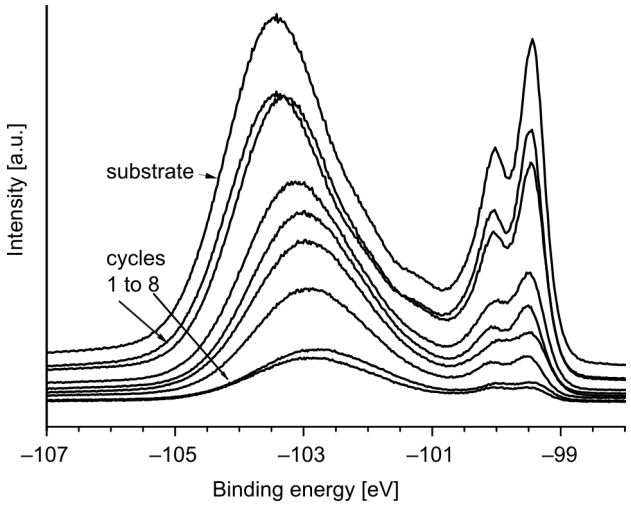

Fig. 1. In-situ growth of HfO_2 on a SiO_2/Si(001) substrate. The Si2p core levels are measured with the photon energy of 150 eV after the initial etch and after 8 consecutive ALD cycles

In Figure 1, we show the Si2p variation for the etched substrate and after 8 successive ALD cycles. The photon energy used to obtain these spectra was 150 eV, i.e. the spectra are very surface sensitive. The resolution was set to about 50 meV, giving the possibility to observe the spin-orbit splitting of the substrate related (Si^{0+}) component of the Si2p at about 99.6 eV, which is about 0.6 eV. Also, the intermediate oxidation components (Si^{+1}, Si^{+2}, and Si^{3+}) can be observed at binding energies between 100 eV and 103 eV. The intensities of the spectra are divided by the incoming photon flux, which is a function of the residence time in a synchrotron.

In Figure 2, we report on the corresponding NEXAFS spectra at the Si2p edge, measured in the photon energy range from 95 eV to 120 eV. Also, here, the intensities of the absorption spectra were divided by the incoming photon flux, because of the time dependence and, in this case, the photon energy dependence.

By increasing the deposition of HfO_2, the overall intensity of the Si2p core level changes because of the increasing thickness of the oxide. Electrons from the substrate have to travel into the Hf-oxide film before escaping into the vacuum. The elastic scattering of those electrons produce an intensity attenuation which is exponentially dependent on the overlayer thickness d as expressed in the equation $I = I_0\exp(-\lambda/d)$, where λ represents the mean free path of the electrons in the oxide. This is a function of the electron kinetic energy, with a minimum at about 0.5 nm for electrons with

a kinetic energy of 50 eV. It is therefore possible to determine the thickness of the oxide film through the intensity weakening of the Si oxide and the substrate components.

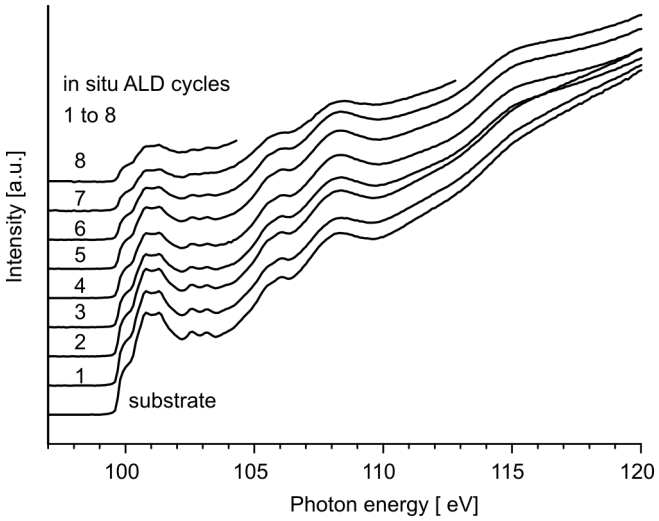

Fig. 2. In-situ growth of HfO_2 on a SiO_2/Si(001) substrate. The total electron yield spectra are taken at the Si2p edge of the sample after the initial etch and after every ALD cycle.

In Table 1, we report the Hf-oxide thickness extracted from the photoemission data after every cycle. The estimation was made by considering a homogenous oxide layer and by adopting the value 0.5nm for the mean free path of the electrons with a kinetic energy of about 50 eV in HfO_2. The simple assumption of a homogeneous oxide layer could be misleading for the interpretation of our results, as in the ALD growth the coverage of the surface is not necessarily homogeneous. Nevertheless, we are developing a mathematical model to take into account the deviation of the experimental results from a simplified homogeneous growth.

Table 1. Thickness of the initial SiO_2 and of the HfO_2 as determined from the XPS intensities after every ALD cycle

Film	Etched SiO_2	HfO_2							
		1 cycle	2 cycles	3 cycles	4 cycles	5 cycles	6 cycles	7 cycles	8 cycles
Thickness [nm]	0 .54	0.13	0.20	0.53	0.69	0.86	1.06	1.49	1.62

After the 8th cycle the substrate is covered with a Hf-oxide film about 1.5 nm thick, showing an excellent sensitivity of our technique to films with a thickness in the nanometer range. At such a thickness, the contamination of the sample due to the transport in air certainly would considerably distort the interpretation of the experi-

mental data. However, with our in situ facility, we can assure the measurement of thickness and analyze the chemical state after each cycle.

The Si2p photoemission spectra change also in shape with increasing HfO_2 deposition. This is especially evident in the energy range between 102 eV and 104 eV, where the contributions from Si^{3+} and Si^{4+} are expected. In the etched sample, the most intense peak is centred at 103.4 eV due to the Si^{4+} component from SiO_2. After the first three cycles, the peak shifts evidently towards lower binding energies, meaning an increase of the Si^{3+} component. After the first three cycles the shift is still present up to the 6th cycle but is much smaller, and it is undetectable in the last two cycles. The strong shift observed in the first cycles is due to the formation, during the early stages of the growth, of Hf-silicate (Hf–O–Si bonds), while in the next cycles the growth is converted to HfO_2. Also here, the observation of the transition between the Hf silicate growth and the HfO_2 growth were possible only because the sample was transferred into the measurement chamber without breaking the vacuum and without contaminating it with external agents.

Also the NEXAFS spectra recorded at the Si2p edge show variations with the growth of Hf oxide. The two main structures are those between 100 eV and 105 eV, ascribed to the substrate Si, and those between 105 eV and 115 eV, derived from SiO_2. The oxide growth induces an attenuation of the absorption spectra in a similar way as for the photoemission spectra. Anyway, the attenuation observed in the energy range of the substrate Si is slightly different from that observed in the energy range of SiO_2. That deviation could be due to either formation of an extra silicon oxide during the Hf oxide deposition or to the transformation of the initial SiO_2 into Hf silicate. The latter possibility is in accordance with the broadening of all peaks in the range 105–115 eV due to smearing of the silicate signal into the silicon dioxide one. From the present status, no definitive answer can be given, but more accurate measurements, at the O1s edge for example, should clarify this point.

3.2. Band gap determination by combined XAS and RIXS measurements

In this section, we report on a study of a hidden layer of AlON deposited between the Si(001) substrate and a Pr_2O_3 layer. In the particular sample used for the studies, the thickness of the AlON layer was 1.5 nm, and the thickness of the Pr_2O_3 layer was 5 nm. The AlON films were prepared by reactive ion sputtering from an Al target; details have been published elsewhere [19]. Pr_2O_3 films were obtained by thermal evaporation in an e-beam evaporator; for details see [15].

In Figure 3, the resonant inelastic X-ray spectroscopy (RIXS) data are shown obtained by excitation above the N1s edge. In a RIXS spectrometer (also called X-ray emission spectroscopy XES), upon resonant excitation, the emitted X-ray fluorescence photons are collected and recorded in function of their detected energy. This method yields a partial density of states of the valence band. Photons of 405 eV were used to excite emission and the emitted photons in the energy range between 370 eV and

400 eV were collected. The observed bands correspond to the N2p valence states in the hidden AlON layer. The triple shaped valence features are very similar to the valence band features of other 2p systems such as O2p in SiO_2 or C2p in C-based compounds reported by RIXS as well as by XPS valence band studies.

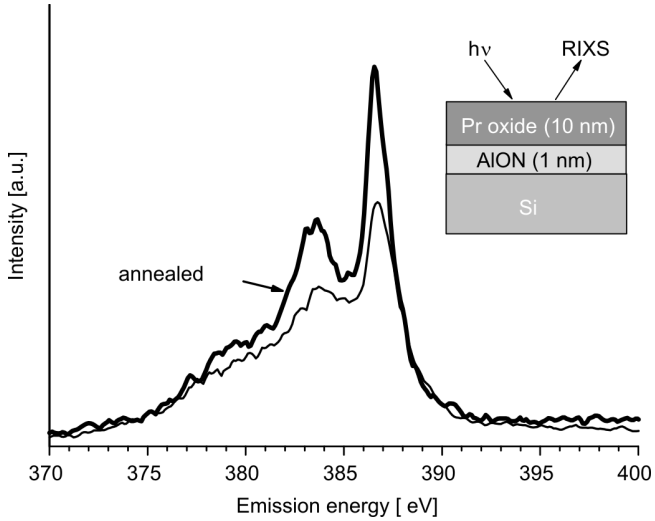

Fig. 3. RIXS spectrum taken at the resonant excitation (405 eV) from a hidden AlON layer in a Pr_2O_3/AlON/Si sandwich structure. Thin line: as deposited sample, bold line: sample annealed at 800 °C, 10 min in nitrogen

In Figure, 3 two spectra are shown. One spectrum is obtained from a sample where the AlON–Pr oxide stack was investigated as prepared, while the other curve is from a sample taken out of the same run but after annealing the stack at 800 °C for 10 min in nitrogen. The difference in the data indicates that upon annealing some crystallites within the Pr oxide film form causing a reduction of the film thickness. Consequently, the N1s signal from the hidden AlON layer appears stronger in the annealed sample. Another difference is very evident: in the annealed sample the valence features appear more sharpened. Another difference is also very evident: in the annealed sample the valence features are more sharply profiled. This is an argument which indicates some ordering in the otherwise more amorphous layers right after the sputtering deposition.

For a further analysis of the RIXS data in Fig. 4 we have used the spectrum of the annealed sample but now have included the XAS spectrum recorded on an AlON film before depositing the Pr_2O_3 layer. The purpose of this figure is to combine the valence band state density with the density of the empty conduction band states. In addition, we have marked the position of the Fermi energy which we obtained from independent measurements of metallic systems.

As a consequence, these combined data may be used to derive a band gap value for the hidden AlON buffer layer. A value of ca. 7 eV was determined and that value

considers only the N2p derived partial density of states. It should be mentioned that our results are taken upon resonant excitation and we therefore probe selectively only the N2p states. However, with this value we have demonstrated that our choice to use AlON as a buffer material is quite reasonable. The band gap is smaller than that of Al_2O_3 (ca. 9 eV) but still large enough to ascertain a proper dielectric behaviour of that buffer layer. The band offset with respect to the Si-substrate amounts to 4 eV for the VB and 2 eV for LB.

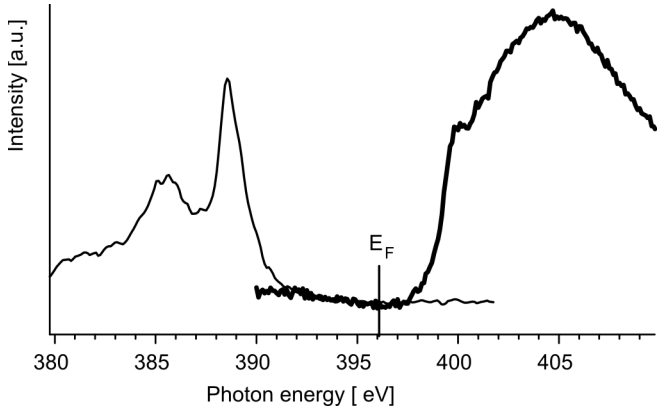

Fig. 4. Combined RIXS (thin line) and XAS (bold line) data from AlON layers plotted on a common energy scale which is referred to the Fermi energy

Determining the VBM from the slope of the sharp feature yields the value of ca. 5 eV below E_F. However, there are still some states appearing above that value. These states are due to hybridization of the N2p levels with the oxidic valence states. In Pr_2O_3 films the value of the VBM is about 3 eV below E_F. This is in agreement with the width of the hybridized states shown in Fig. 4.

To summarize, in this section we demonstrated the combination of RIXS and XAS data upon resonant excitation to obtain the partial density of states for both the valence and conduction bands. In addition, if the position of the Fermi energy can be obtained from independent measurements, the absolute values of the valence band maximum and of the band gap of the investigated system can be derived. Furthermore, we have demonstrated that the use of X-ray fluorescence spectroscopy enables the analysis of hidden layers with sufficient data quality.

3.3. Improved electrical parameters by using an aluminum oxynitride (AlON) buffer layer

Chemical reactivity of the Pr_XO_Y/SiC and Pr_XO_Y/Si interfaces causes a deleterious interaction yielding graphite and silicate formation after direct deposition of Pr_XO_Y onto SiC and Si, respectively [9, 17]. This leads to high leakage currents [4] and it limits the reduction of the CET as well.

Using an approximately 1–1.5 nm thick buffer layer of AlON, we found leakage current values improved by several orders in comparison to the stacks without the buffer. At a CET of 4 nm we could observe a leakage current density of 10^{-7} A/cm^2 (at 1 V above flat band condition) on silicon based stacks (Pr_XO_Y/AlON/Si). Furthermore, we found, for this system, that the introduction of the AlON buffer layer combined with subsequent annealing in nitrogen at 800 °C results in a decrease of the density of interface states D_{it}. Values of 5×10^{11}–1×10^{12} eV$^{-1}\cdot$cm^{-2} are observed. Using a plot of the CET versus the physical thickness of Pr_XO_Y and fitting it to a simple model of capacitors in series, we can deduce the thickness of an interfacial layer and the permittivity values of the high-*k* material. Permittivity values of the high-*k* material in the range of 17–20 were calculated in this way, the values are not influenced significantly by the buffer layer. But we could also show that the interfacial layer CET value could be reduced from 3.9 nm to 1.3 nm by using the AlON buffer, where we have to point out that this value already contains the buffer layer CET value, so the unintentional interfacial layer thickness is even smaller. Also on SiC the insertion of the buffer layer leads to better electrical characteristics. For further details of these investigations refer to [4, 19, 20].

Summarizing this section, AlON provides a suitable buffer layer between high-*k* Pr_XO_Y and Si as well as between Pr_XO_Y and wide band gap SiC. This is evident from our spectroscopic investigations (reduced silicon out-diffusion [20], higher Pr_2O_3 fractions [20], stable interface [18]), and from improved electrical parameters (low values of leakage current, D_{it}, and interfacial layer thickness). A better band alignment and reduced interfacial reactions might be responsible for these improvements.

4. Characterization of organic materials

In this paragraph, the use of synchrotron radiation (SR) based spectroscopic and microscopic techniques is demonstrated for the analysis of organic materials. We present data from a ferroelectric polymer which is a candidate for non-volatile memory devices, and we report on studies of fullerene based thin films which may be used as low-*k* materials.

4.1. Ferroelectric polymer P(VDF-TrFE)

Non-volatile ferroelectric polymer random access memory devices based on ferroelectric polymers have the potential to overcome many of the fabrication issues faced in the inorganic semiconductor industry [24]. Ferroelectric properties of copolymers of vinylidene fluoride with trifluoroethylene (P(VDF-TrFE)) have become of great interest due to potential use in non volatile memory technology [25]. It was found that in a compositional range from 50/50 to 80/20 mol % ratio of VDF/TrFE, copolymers have ferroelectric phase at room temperature [26]. In addition, these copolymers are

soluble in non toxic reagents. The most common solvent for preparing P(VDF-TrFE) thin films is 2-butanone, or cyclohexanone [27, 28]. The P(VDF-TrFE) solution is available for spin coating, ink jet printing, or roll to roll printing [29]. Spin cast films of P(VDF-TrFE) are not only available as a ferroelectric material but also usable as an organic high-*k* insulation for organic transistors [30, 31].

For electrical contacts, thermally evaporated aluminium has been widely used, compared with other metals such as Cu or Ag, because of its good adhesive strength on the copolymer film [32, 33]. But due to interactions at the interface, even at room temperature, a thin layer of AlF_3 is formed. If poly (3,4-ethylenedioxydi-thiophene):poly(styrenesulfonic acid) (PEDOT:PSS) is used, no interface reaction takes place, as revealed by XPS [34-36].

Here, we like to focus on some fundamental investigations of the copolymer molecular structure, performed by polarization dependent X-ray absorption spectroscopy (XAS) at the U49/2-PGM beam line of the BESSY-II synchrotron. As a copolymer, we used P(VDF-TrFE) in mol% ratio of 70:30, delivered by Piezotech S.A., France. The solvent was 2-butanone, the substrate a Si(100) wafer covered with PEDOT:PSS to prevent possible interface reactions. After spin coating, the copolymer film was annealed for 2 h at 135 °C to improve crystallinity [37].

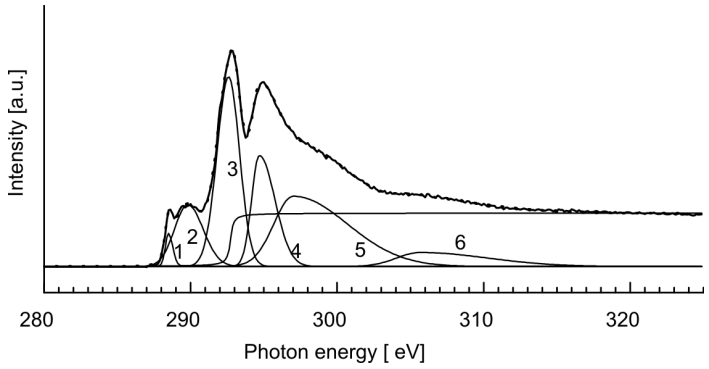

Fig. 5. C-K edge XAS spectra of a thick P(VDF-TrFE) film (~ 100 nm) on SiO_2/Si(100). Details of the peak deconvolution are given in the text

Figure 5 shows the results of XAS measurement of a thick copolymer film (100 nm, measured with a profilometer). The C-K edge is shown in the photon energy range from 280 eV to 325 eV, where various peaks can be isolated by a curve fitting procedure [38]. The peaks 1 and 2 at 287.2 eV and 289 eV are due to a σ^*(C–H) resonance, the peak 3 at 292 eV has to be attributed to a σ^*(C–F) resonance, and the peaks 4, 5, and 6 above 294 eV should be due to σ^*(C–C) resonances [38, 39]. The π^* resonances are not observed as the P(VDF-TrFE) copolymer does not contain unsaturated C–C bonds. It is also evident that no beam damage of the copolymer thin film occurred.

In Figure 6, The C-K edge of a thin copolymer film is shown. The film of the thickness of about 0.4 nm was deposited again on the PEDOT:PSS/Si(100) substrate.

This copolymer film thickness was measured by the attenuation of the XPS signal of PEDOT:PSS [34] and corresponds to the thickness of one monolayer (0.5 nm) [40].

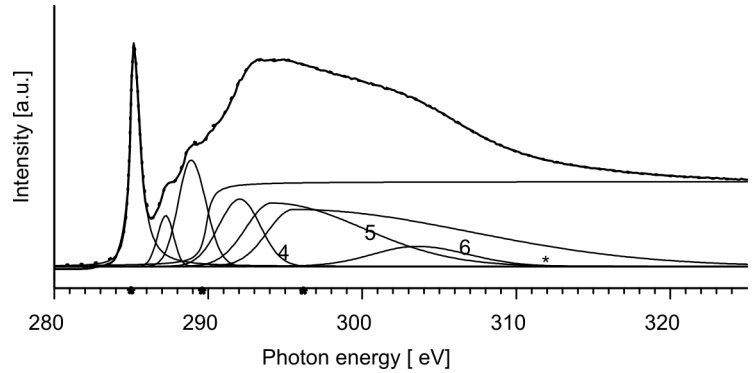

Fig. 6. C-K edge XAS spectra of very thin P(VDF-TrFE) film (ca. 0.4 nm) on PEDOT:PSS SiO_2//Si(100). For details of the peak deconvolution refer to the text. Peaks marked by a star are attributed to the substrate

Obviously, now there is a very sharp peak at 285.0 eV, which is due to π^*(C=C) resonances of PEDOT:PSS. This signal is not observed for the thicker film in Fig. 5 as it is attenuated by the PVDF film. The peak at the photon energy of 287.2 eV is due to a σ^*(C–H) resonance, and the peak at 288.9 eV is again attributed to the substrate with the σ^*(C–S) resonance of PEDOT:PSS. The rest of the peaks are only identifiable by a curve fitting procedure (see figure 6). In the curve fitting procedure, the π^*(C=C) resonance fits to Gaussian profile which match the height of the experimental peaks.

The Gaussian function matched well because of the limitation of instrumental resolution, while the Lorentzian fit is poor because the base is too broad [38]. If the instrumental resolution is comparable with the intrinsic lifetime-related width of the peak, then the peak is fitted by a Lorentzian profile. In our spectra, the σ^*(C–H), σ^*(C–S), and σ^*(C–F) resonances are fitted with Lorentzian profiles. The other peaks are fitted with an asymmetric Gaussian profile. The increase in width of resonances with increasing energy can be simply attributed to lifetime broadening. That means, the higher the energy of the final state, the shorter its lifetime and hence the broader the peaks [41, 42]. In addition to the peaks, near edge spectra of XAS contain one or sometimes more step-like features referred to as continuum steps. These steps are the result of the excitation of the core electron to a continuum or quasi-continuum of final states, e.g. to the smooth density of states [38].

Based on this peak identification, we present an analysis of angle dependent linear dichroism. In order to understand the ferroelectric nature of the PVDF copolymer the existence of oriented dipoles is a question of special interest. Here, we show an analysis of our NEXAFS measurement of an ultrathin (0.4 nm) copolymer film deposited on a PEDOT:PSS/Si substrate. Due to linear dichroism, we have to expect a modula-

tion of the intensity of specific absorption signals, if they can be attributed to a preferred orientation of dipole moments inside the copolymer film. In such cases, using the dipole approximation, this intensity should be proportional to $\cos^2\theta$, if an idealized alignment of the dipoles perpendicular to the surface is assumed [38]. In our experiment, the angle θ is the angle between the direction of the incident beam and the normal to the surface of the sample (inset in Fig. 7).

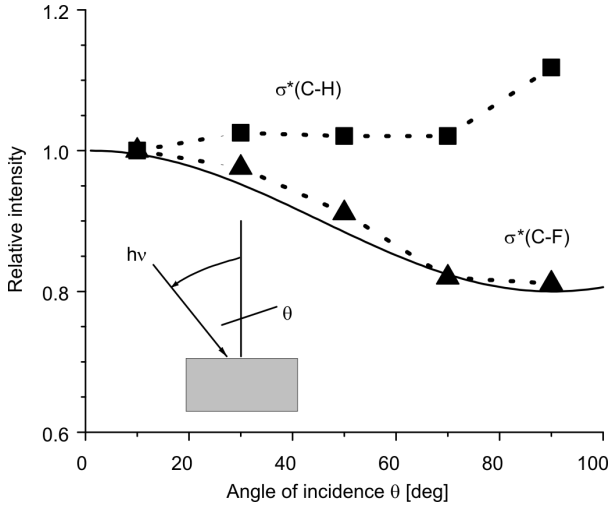

Fig. 7. Angle dependent spectra of P(VDF-TrFE) on a PEDOT/Si(100) substrate, 0.1 wt. % P(VDF-TrFE) in 2-butanone (thickness ca. 0.4 nm); the intensities of the σ^* (C–F) excitation at 292.04 eV (triangles, dotted line) and of the σ^* (C–H) excitation at 287.28 eV (squares, dotted line) normalized to the value at near-normal incidence (10°). The solid line presents the $\cos^2\theta$ modulation of intensities for an idealized alignment of dipoles (100% perpendicular to the surface of the substrate)

In Figure 7, we show the intensity of the σ^*(C–F) resonance at 292.04 eV compared with the σ^*(C–H) excitation at 287.28 eV. The observed intensity values are normalized to the peak intensity at 10°. For the σ^*(C–F) excitation (the C–F dipole) clearly an angular dependence of the intensity is visible. In contrast, for the σ^*(C–H) excitations we have no angular dependence at all. The highest dipole moment has to be attributed to the σ^*(C–F) resonance, caused by the electronegativity of fluorine atoms. Consequently we assign the σ^*(C–F) excitations to represent the ferroelectric dipole moments while the σ^*(C–H) excitations have no contribution to the ferroelectric moments, as expected. The observed angular variations can be modelled according to $I = 0.2\cos^2\theta + 0.8$ with a reasonable agreement. This means that about 20% of the ferroelectric dipoles are oriented with respect to the polarization of the incoming light. This quantity is remarkable as we have not applied an external field to the film. The $\cos^2\theta$ dependence certainly is just an approximation. Nevertheless, the measurements show a clear linear dichroism indicative of an alignment of C–F dipoles, even without the application of an external field. It seems that self alignment and ferroelectric order-

ing occurs even for ultrathin and spin-coated films, if we avoid reactive interfaces and use an inert substrate such as PEDOT:PSS.

4.2. Fullerene thin films as low-*k* materials

The low-*k* materials investigated so far include examples from organosilicate glasses (OSG) and of fullerene based porous ultra low-*k* (ULK) films. OSG materials that are used as low-*k* materials to isolate on-chip interconnects are investigated and we use the chemical sensitivity of the X-ray absorption signal around the C1s and Si2p edges to describe the chemical stability of such materials against UV curing and plasma treatment. In our XAS studies we are able to distinguish the individual σ-orbitals based on the C1s absorption features, i.e. the bonds of individual groups of the material investigated. In general, in the data for OSG the C–C, the C–O, and the C–H groups can be identified by different transition energies of the corresponding excitations. If one of the groups is modified, only this particular contribution of the XAS spectrum changes, which makes the technique very sensitive and selective for analysis of materials.

For fullerene based polymers, being candidates for ultra low-*k* materials [43], we demonstrate the stability of fullerene complexes after incorporation in sol-gel processed films. In the case of C_{60} derived components, there is a particular mechanism causing a characteristic feature in the absorption data. Based on the electronic properties of the C_{60} molecules in all C_{60} derived compounds, there is a characteristic split in the lowest absorption band causing a three-peak structure.

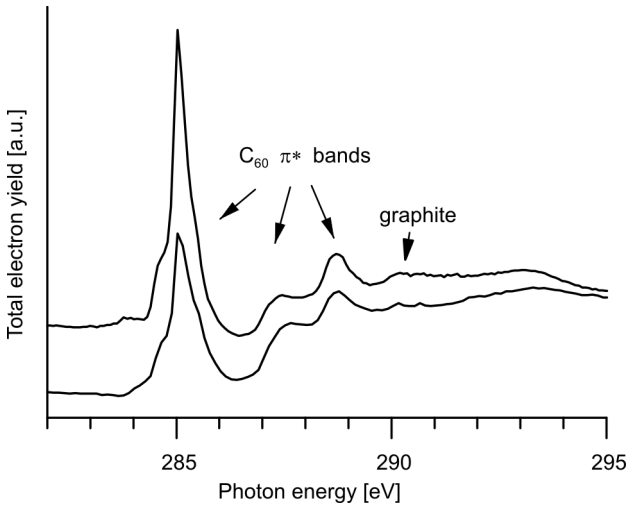

Fig. 8. XAS spectrum at the C1s edge of a thin film of a fullerene based low-*k* material taken at two different positions of the sample

These features represent transitions into the triple π^* orbitals of C_{60} and range between 285 eV and 289 eV. In Fig. 8 we show the total electron yield (TEY) spectra of

C_{60} derived films in the energy range between 282 eV and 295 eV. In line with expectation, we find the characteristic features of the C_{60} molecule are well pronounced and resolved for these C-cage ULK films. The observed features peak around 285 eV, 287.8 eV, and around 289 eV. In particular, the middle band appears at a higher transition energy than in pure C_{60} films. We attribute the differences in the peak position to the specific bonding of the C_{60} polymer.

Still, we have problems in recording such data. The films seem to be inhomogeneous and our spectroscopic observations indicate that at some positions there is a higher content of graphite in the films. In previous ULK films the amount of graphite was even larger and this made a clear detection of the split π^* bands almost impossible.

We have also investigated the XAS data of the preliminary obtained C-cage based ULK films at the N1s and O1s edges, respectively. At the N1s we identified absorption features that we attribute to residuals of the solvents used for the preparation of the films. At the O1s edge we find very unusual features, as there is a sharp absorption band at 531 eV which is well separated from the main absorption band rising at around 537 eV. Such an absorption pattern is usually observed for conducting oxides such as NiO and CrO_2.

5. Summary

We demonstrated some recent examples of synchrotron radiation based analysis of materials. We report on XPS, XAS, and RIXS studies on HfO_2 thin films and on Pr_2O_3 /AlON/SiO_2 multilayer stacks. The SR based techniques are used to learn about the growth mechanism, chemical stability, and interface reactions in such systems. In addition, the electronic properties such as the band-offsets and the band gap, are determined, as demonstrated, for the latter system.

For organic systems, we report on the usage of the linear dichroism in the absorption signal to learn about the existence of ferroelectric dipole moments in such films. Finally, the fine structure of the absorption spectra at the C1s edge is used, in particular, for detailed analysis of the composition of films. As a specific example, it is shown how this method can be used to identify C_{60} building blocks of a polymer which is to represent an ultralow-*k* prototype material.

Acknowledgements

We would like to acknowledge the skillful assistance of G. Beuckert, I. Paloumpa, and P. Hoffmann. This work was supported in part by the DFG SPP 1157 (SCHM 745/11-1-2 and SCHM 745/9-1-3) and BMBF (13N9431).

References

[1] SCHMEISSER D., HOFFMANN P., BEUCKERT G., *Electronic Properties of the Interface formed by Pr_2O_3 growth on Si(001), Si(111) and SiC(0001) surfaces* [in:] *Materials for Information Technology,*

Devices, Interconnects and Packaging, *Series: Engineering Materials and Processes*, E. Zschech, C. Whelan, T. Mikolajick (Eds.), Springer, Berlin, 2005, 449–460.
[2] SCHMEISSER D., ZHENG F., HIMPSEL F.J., ENGELMANN H.J., ZSCHECH E., Mat. Sci. Semicond. Proc., 9 (2006), 934 – 939.
[3] SCHMEISSER D., ZHENG F., PEREZ-DIESTE V., HIMPSEL F.J., LONIGRO R., TORO R.G., MALANDRINO G., FRAGALÀ, I.L., Mater. Sci. Eng., C 26 (2006), 1122.
[4] HENKEL K., TORCHE M., SOHAL R., SCHWIERTZ C., HOFFMANN P., SCHMEISSER D., MRS Proceedings, 911 (2006), B10-11.
[5] LUPINA G., SCHROEDER T., DABROWSKI J., WENGER CH., MANE A.U., MÜSSIG H.-J., HOFFMANN, P., SCHMEISSER D., J. Appl. Phys., 99 (2006), 114109.
[6] SCHMEISSER D., LUPINA G., MÜSSIG, H.-J., Mater. Sci. Eng., B 118 (2005), 19.
[7] SCHMEISSER D., MÜSSIG H.-J., *Pr-silicate formation on SiO_2 covered 3C–SiC(111),* AIP Conference Proceedings, 772 (2005), 75.
[8] LUPINA G., SCHROEDER T., DABROWSKI J., WENGER CH., MANE A.U., LIPPERT G., MÜSSIG H.-J., HOFFMANN P., SCHMEISSER D., Appl. Phys. Lett. 87 (2005), 092901
[9] GORYACHKO A., PALOUMPA I., BEUCKERT G., BURKOV Y., SCHMEISSER D., Phys. Stat. Solidi, C 1 (2004), 265 – 268.
[10] SCHMEISSER D., Mater. Sci. Semicond. Proc., 6 (2003), 59.
[11] SCHROEDER T., LUPINA G., SOHAL R., LIPPERT G., WENGER CH., SEIFARTH O., TALLARIDA M., SCHMEISSER D., J. Appl. Phys., 102 (2007), 014103.
[12] HOFFMANN P., GORYACHKO A., SCHMEISSER D., Mater. Sci. Eng., B 118 (2005), 270.
[13] SCHMEISSER D., MÜSSIG H.-J., Solid State Electronics, 47 (2003), 1607.
[14] SCHROEDER T., LUPINA G., SOHAL R., LIPPERT G., WENGER CH., SEIFARTH O., TALLARIDA M., SCHMEISSER D., J. Appl. Phys., 102 (2007), 014103.
[15] TORCHE M., HENKEL K., SCHMEISSER D., Mater. Sci. Eng., C 26 (2006), 1127.
[16] SCHMEISSER D., MÜSSIG H.-J., J. Phys. Cond. Matter, 16 (2004), 153.
[17] SCHMEISSER D., MÜSSIG H.-J., DABROWSKI J., Appl. Phys. Lett., 85 (2004), 88.
[18] SOHAL R., TORCHE M., HENKEL K., HOFFMANN P., TALLARIDA M., SCHMEISSER D., Mater. Sci. Semicond. Proc., 9 (2006), 945.
[19] HENKEL, K., SOHAL R., SCHWIERTZ C., BURKOV Y., TORCHE M., SCHMEISSER D., MRS Proc., 996 (2007), H05-23.
[20] HENKEL K., KARAVAEV K., TORCHE M., SCHWIERTZ C., BURKOV Y., SCHMEISSER D., J. Phys.: Conf. Ser., 94 (2008) , 012004.
[21] NICOLLIAN E.H., BREWS J.R., *MOS Physics and Technology,* Wiley, New York, 1982.
[22] MACK P., WHITE R.G., WOLSTENHOLME J., CONARD T., Appl. Surf. Sci. 252 (2006), 8270.
[23] DELABIE A. ET AL., J. Electrochem. Soc., 153 (2006), F180.
[24] FORREST S.R., Nature, 428 (2004), 911.
[25] PARASHKOV R., BECKER E., RIEDL T., JOHANNES H., KOWALSKY W., Proc. IEEE 93 (205), 1321.
[26] ZHANG Q.M., XU H., FANG F., CHENG Z.-Y., XIA F., YOU H., J. Appl. Phys., 89 (2001), 2613.
[27] NABER R.C.G., BLOM P.W.M., MARSMAN A.W., DE LEEUW D. M., Appl. Phys. Lett., 85 (2004), 2032.
[28] NABER R.C.G., DE BOER B., BLOM P.W.M., DE LEEUW D.M., Appl. Phys. Lett., 87 (2005), 203509.
[29] ZHANG S., LIANG Z., WANG Q., ZHANG Q., Mater. Res. Soc. Symp. Proc., 889 (2005), W05-02.1.
[30] MÜLLER K., PALOUMPA I., HENKEL K., SCHMEISSER D., J. Appl. Phys., 98 (2005), 056104.
[31] MÜLLER K., PALOUMPA I., HENKEL K., SCHMEISSER D., Mat. Sc. Eng., C 26 (2006), 1028.
[32] XIA F., ZHANG Q.M., Appl. Phys. Lett., 85 (2004), 1719.
[33] WU P., YANG G.-R., MA X. F., LU T.-M., Appl. Phys. Lett., 65 (1994), 508.
[34] MÜLLER K., MANDAL D., SCHMEISSER D., MRS Proc., 997 (2007), I6-02.
[35] MÜLLER K., MANDAL D., SCHMEISSER D., Thin solid films, submitted.

[36] MÜLLER K., BURKOV Y., MANDAL D., HENKEL K., PALOUMPA I., GORYACHKO A., SCHMEISSER D., Physica Status Solidi (A) 205 (2008), 600 – 611.
[37] FURUKAWA T., Phase Transitions, 18 (1989), 143.
[38] STÖHR J., NEXAFS Spectroscopy, 2nd ed. Springer, Berlin, 2003.
[39] JOLLY W.L., BOMBEN K.O., EYERMANN C.J., At. Data Nucl. Data Tables, 31 (1984), 433.
[40] PALTO S., BLINOV L., DBOVIK E., FRIDKIN V., PETUKHOVA N., SOROKIN A., VERKHOVSKAYA K., YUDIN S., ZLATKIN A., Europhys. Lett., 34 (1996), 465.
[41] DEHMER J. L., DILL D., WALLACE S., Phys. Rev. Lett., 43 (1979), 1005.
[42] SETTE F., STÖHR J., HITCHCOCK A.P., J. Chem. Phys., 81 (1984), 4906.
[43] ZAGORODNIY D., CHUMAKOV D., TÄSCHNER C., LUKOWIAK A., STEGMANN H., SCHMEISSER D., GEISLER H., ENGELMANN H.J., HERRMANN H., ZSCHECH E., IEEE Trans. Semicond. Manuf., 21 (2008), 646.

Received 15 January 2008
Revised 19 December 2008